2

Functionalized halloysite nanotubes for enhanced removal of lead(II) ions from aqueous

solutions

5

Salvatore Cataldo[a], Giuseppe Lazzara[a], Marina Massaro[b], Nicola Muratore[a], Alberto Pettignano[a*],

Serena Riela[b*]

[a] Dipartimento di Fisica e Chimica, Università di Palermo, Viale delle Scienze, I-90128 Palermo,

Italy

[b] Dipartimento di Scienze e Tecnologie Biologiche, Chimiche e Farmaceutiche. Università di

Palermo, Viale delle Scienze, I-90128, Palermo, Italy

12

* Corresponding authors: Tel: +39-091-23897959

E-mail addresses: alberto.pettignano@unipa.it; serena.riela@unipa.it

15

ABSTRACT

In this study, environmental friendly halloysite nanotubes and their amino derivatives were used as

adsorbent materials for lead(II) ions. The adsorption ability of both nanomaterials towards Pb^{2+} ions

has been studied in $NaCl_{aq}$, at $I = 0.1$ mol L^{-1}, in the pH range 3 – 6. Moreover, the effect of ionic

strength on the adsorption process was evaluated at the pH of maximum efficiency of the adsorbent

materials. Kinetic and equilibrium experiments were carried out by using the Differential Pulse

Anodic Stripping Voltammetry (DP-ASV) technique to check the metal ion concentration in

solution after contact with the two adsorbents. Different isotherm and kinetic equations were used

to fit the experimental data. The speciation of metal ion and the characterization of the adsorbents

with different techniques were considered in order to establish the suitable experimental conditions

for the metal ion removal. The collected data showed that the functionalization of halloysite

27 enhances the adsorption ability of the clay mineral and it makes the nanoclay a good candidate for

28 metal removal from aqueous solutions.

29

30

31

32 1. Introduction

33 Industrial and agricultural activities, together with vehicle traffic emission, are the main causes of

34 heavy metals pollution. Toxic metals are persistent in the environment and accumulate in terrestrial

35 and aquatic ecosystems with serious consequences for human health (Förstner et al., 1995). Among

36 them, lead is considered one of the most toxic towards living organisms and a long term exposure

37 can cause a serious damage to different organs and disease of cardiovascular, nervous and immune

38 systems. (Mason et al., 2014; Gidlow, 2015)

39 During the last decade various nanomaterials are extensively used in the heavy metal ions removal

40 from aqueous solutions or from soils. Among them, clay minerals have gathered particular interest

41 owing to their unique features such as, high specific surface area, low toxicity and natural

42 availability at low price (Dong et al., 2012; Cataldo et al., 2015). Halloysite nanotubes (Hal) are

43 particular clay minerals with a predominantly hollow tubular structure (Joussein et al., 2005). Hal

44 are chemically similar to the platy kaolin and possess a peculiar chemical composition of the

45 surfaces. They consist in 10-15 aluminosilicate layers with an external surface constituted by

46 siloxane groups and an inner lumen composed of aluminol groups. Owing to this peculiar

47 composition, Hal are positively charged in the interior whereas a negative charge is present on the

48 external surface in a wide pH range. This charge separation is related to the acid-base properties of

49 functional groups of Hal studied in a recent article (Bretti et al., 2016). The different surface

50 chemistry allows to the selective functionalization at the inner or outer side making possible the

51 synthesis of several nanomaterials with hierarchical nanostructure (Cavallaro et al., 2014). The

52 covalent modification of the outer surface is most commonly achieved by grafting silanes via

53 condensation between hydrolyzed silanes and the surface hydroxyl groups of the Hal located on the
54 edges or on external surface defects (Yuan et al., 2008; Yuan et al., 2012; Tan et al., 2016; Sabbagh
55 et al., 2017). According to Yuan et al. the Al-OH groups present in the Hal lumen possess high
56 degree of chemical reactivity towards organosilane. On the contrary, the external surface of Hal
57 nanotubes consists of siloxane (Si-O-Si) groups and few silanols (Si-OH). However, due to the
58 presence of some surface defects more hydroxyl groups exist on the surface of Hal nanotubes.
59 These hydroxyl groups are the potential reactive sites for the surface modification on the external
60 surface of Hal nanotubes which increased the interaction of organosilanes with Hal nanotubes
61 (Yuan et al., 2008) as reported by other authors (Rawtani et al., 2017; Sadjadi and Atai, 2018).

62 The functionalization of Hal surfaces opens up several application fields, where halloysite hybrids
63 can be successful applied. Therefore, functionalized halloysite was used as filler for polymer or
64 hydrogel matrices (Liu et al., 2010; Fan et al., 2013; Silva et al., 2013), drug carrier and delivery
65 (Lvov et al., 2015; Liu et al., 2016; Lvov et al., 2016; Massaro et al., 2016a), catalyst support
66 (Massaro et al., 2016b) as well as adsorbent (Peng et al., 2015). In this context Hal have been
67 considered ideal alternatives for the preparation of adsorbents for removal of different kinds of toxic
68 metal ions or organic contaminants from wastewaters or from polluted soils (Zhao et al., 2013;
69 Kurczewska et al., 2015; Maziarz et al., 2015; Hebbar et al., 2016; Matusik, 2016; Meng et al.,
70 2016; Zeng et al., 2016; Zhu et al., 2017). Indeed, respect to other nanoclay, the possibility to
71 adsorb pollutants both in Hal lumen and on Hal external surface, increases the removal efficiency
72 (Zhao et al., 2013).

73 Generally, pristine Hal (p-Hal) can remove heavy metal ions from aqueous media through the
74 mechanisms of site geometry, physical and/or chemisorption and so on. However, application of
75 these materials as adsorbents of pollutants is limited by their low loading capacity, less metal ion
76 binding active-sites, and low selectivity to specific metals. (Zhu et al., 2017) To enhance the
77 loading capacity and the affinity toward heavy metal ions, p-Hal can be functionalized with some
78 interesting nanomaterials and/or functional groups to endow them with the extra mechanism of

79   complexation (Matusik, 2014; Massaro et al., 2017). Zhu et al. (Zhu et al., 2017) reported the

80   synthesis of a new nanoadsorbent based on Hal for the simultaneous removal of Cr(VI) and Sb(V)

81   from wastewater. In order to improve heavy metal adsorption efficiency halloysite was also

82   functionalized with hexadecyltrimethylammonium bromide. The as prepared adsorbent was applied

83   to remove Cr(VI) from aqueous solution showing faster adsorption rate and higher adsorption

84   capacity.(Jinhua et al., 2010)

85   With the final goal to obtain good adsorbent for toxic metal ions herein we report a thorough study

86   of the amino functionalized halloysite (Hal-NH$_2$) adsorption ability towards Pb^{2+} ions. FT-IR, TGA

87   and SEM techniques and contact angle measurements were used to characterize the adsorbent

88   material whilst Differential Pulse Anodic Stripping Voltammetry (DP-ASV) technique was used to

89   check the metal ion concentration in solution during the batch kinetic and thermodynamic

90   adsorption experiments. A speciation study of p-Hal and of Pb^{2+} ions using literature formation

91   constants (Baes and Mesmer, 1976; Luo and Millero, 2007; Bretti et al., 2016) was done to find the

92   best experimental conditions for the metal ion removal. Sodium chloride was used as background

93   and different ionic strengths were considered in the experiments.

94

95   **2. Materials and Methods**

96

97   *2.1 Reagents.*

98   p-Hal were a commercial product (Sigma, lot MKBQ8631V) and were used after washing with

99   ultra pure water and drying in oven at T = 110 °C. The 3-azidopropyltrimethoxysilane was

100   synthetized as previously reported (Massaro et al., 2016b). NaCl salt (Riedel-de Haën, puriss.) used

101   to set the ionic strength of the solutions at desired values was weighed after drying in oven at 110

102   °C for 2 h. Hydrochloric acid and sodium hydroxide used to adjust the pH of the metal ion solutions

103   were prepared by diluting concentrated Fluka ampoules and standardized against sodium carbonate

104   and potassium hydrogen phthalate, respectively, previously dried in an oven at T = 110 °C. Pb(II)

4

105   ion solutions were prepared by weighing the $Pb(NO_3)_2$ (Aldrich, analytical grade) salt. Standard

106   solutions of Pb(II) ions used for calibration curves were prepared by diluting a 1000 mg L^{-1}

107   standard solution in 2% HNO_3 ($C \pm 0,2\%$ - trace select quality, FLUKA). All the solutions were

108   prepared using freshly, CO_2-free ultra pure water ($\rho \geq 18$ MΩ cm) and grade A glassware.

109

110   *2.2 Synthetic run and characterization of Hal-NH$_2$ nanomaterial*

111   In a typical synthetic run, 4 g of 3-azidopropyl trimethoxysilane were dissolved in 60 mL of dry

112   toluene and 2 g of clay mineral powder were added. The clay mineral was first dispersed under

113   ultrasonic irradiation for 15 min, and then refluxed for 48 h under stirring. Afterwards, the crude

114   solid was filtered off, washed with several aliquots of CH_2Cl_2 and CH_3OH and dried overnight at 80

115   °C under vacuum. The so obtained nanomaterial was re-suspended in DMF and triphenylphosphine

116   (PPh_3) was added to the reaction mixture. The dispersion was left to stir at room temperature for 1h.

117   After this time a NH_3 aqueous solution (2 mL) was added dropwise. After 5 days the solvent was

118   filtered off and the powder was washed several times with CH_2Cl_2 and finally dried at 50 °C under

119   vacuum.

120   Contact angle measurements were performed by using an optical contact angle apparatus (OCA 20,

121   Data Physics Instruments) equipped with a video measuring system having a high-resolution CCD

122   camera and a high-performance digitizing adapter. SCA 20 software (Data Physics Instruments)

123   was used for data acquisition. To obtain a tablet, the powder like material was pressed under 104 kg

124   cm^{-2} for 10 min. The contact angle of water in air was measured by the sessile drop method. The

125   water droplet volume was 10.0 ± 0.5mL. Temperature was set at 25.0 ± 0.1 °C for the support and

126   the injecting syringe as well. Images were collected 25 times per second. From the data analysis the

127   contact angle, the volume and the contact area of the drop were calculated. The volume of the

128   droplet was constant within the time of the experiment.

129 FT-IR spectra in KBr were determined at room temperature in the spectral region 400–4000 cm^{-1} by

130 means of an FT-IR spectrophotometer (Agilent Technologies Cary 630). An average of 30 scans per

131 sample using a nominal resolution of 4 cm^{-1} was registered.

132 The thermogravimetric analysis was performed by means of a Q5000 IR apparatus (TA

133 Instruments) under the nitrogen flow of 25 mL min^{-1} for the sample and 10 mL min^{-1} for the

134 balance. The mass of each sample was ca. 5 mg. The calibration was carried out by means of Curie

135 temperature of standards (nickel, cobalt, and their alloys). The sample was heated from room

136 temperature to 900 °C with a scanning rate of 20 °C min^{-1}. The degradation temperature (T_d) was

137 taken at the maximum of the first order derivative curve of mass loss versus temperature (DTG

138 curves).

139 The microscope ESEM FEI QUANTA 200F was used to study the morphology of the

140 functionalized Hal. Before each experiment, the sample was coated with gold in argon by means of

141 an Edwards Sputter Coater S150A to avoid charging under electron beam.

142

143 *2.3 Procedures for kinetic and thermodynamic experiments*

144 The kinetic experiments for Pb^{2+} ion adsorption by p-Hal and Hal-NH_2 were carried out in NaCl

145 aqueous solution, at $I = 0.1$ mol L^{-1}, in the pH range 3 − 6 and at $T = 25$ °C. ~15 mg of p-Hal or

146 Hal-NH_2 were added to 25 mL of the metal ion solution ($C_{Pb2+} = 30$ mg L^{-1}) placed in a

147 voltammetric cell under constant and regular agitation. The metal ion concentration in solution was

148 measured at various adsorbent/solution contact times in the interval 0 - 360 min. The solution pH

149 was monitored during the experiments.

150 The adsorption isotherm experiments were carried out in the same ionic medium and pH range of

151 kinetic ones, at $I = 0.10$ mol L^{-1} and $T = 25$ °C. Moreover, at pH = 5 the experiments were extended

152 at the ionic strengths 0.25 and 0.5 mol L^{-1}. For each pH and ionic strength, ~ 15 mg of p-Hal or Hal-

153 NH_2 were placed in 9 Erlenmeyer flasks containing 25 mL of Pb(II) solution at different

6

154 concentrations in the range $5 \leq C_{Pb^{2+}} / mg\ L^{-1} \leq 50$. The solutions were stirred at 180 rpm for twelve

155 hours using an orbital mixer (model M201-OR, MPM Instruments) and then were separated from

156 the adsorbent before measuring the pH and the Pb^{2+} concentration.

157 Recycling and reuse experiments were done on the Hal-NH$_2$ material. To this end, ~40 mg of the

158 adsorbent were placed in an Erlenmeyer flask containing 25 mL of Pb(II) solution ($C_{Pb^{2+}} \approx 30$ mg L$^-$

159 ^{1}) in NaCl, at $I = 0.1$ mol L^{-1} and stirred for 6 hours. Then the supernatant was collected for Pb^{2+}

160 analysis. The adsorbent was rinsed with ultra pure water and then treated with 25 mL of HCl 0.1

161 mol L^{-1} to extract the Pb^{2+}. The extractant was separated after 6 hours and collected for Pb^{2+}

162 analysis. The Hal-NH$_2$ was left in NaOH 0.1 mol L^{-1} for 1 hour and then rinsed with ultra pure

163 water and reused. The same procedure was repeated three times.

164 The Pb^{2+} concentration in solutions collected during the experiments was measured by Differential

165 Pulse Anodic Stripping Voltammetry (DP-ASV) technique. The voltammetric apparatus was

166 constituted by a Metrohm 663 VA stand combined with the Autolab potentiostat in conjunction

167 with the IME663 interface. The voltammetric apparatus was controlled by NOVA v. 1.10 software.

168 The VA stand was equipped with a three electrode system consisting of i) a Multi Mode Electrode

169 Pro (Metrohm, code 6.1246.120) working in the Static Mercury Drop Electrode (SMDE) mode, ii) a

170 glassy carbon auxiliary electrode (code 6.1247.000), and iii) a double junction Ag/AgCl/KCl (3 mol

171 L^{-1}) reference electrode (code 6.0728.030). The DP-ASV measurements were performed after

172 bubbling purified N$_2$ gas into the solutions for 150 s. The experimental electrochemical conditions

173 were chosen in order to optimize the quality parameters, as signal/noise ratio, repeatability and

174 accuracy and are reported in Table 1S of Supplementary Materials.

175 Calibration curves of Pb^{2+} ion were done at the same experimental conditions of kinetic and

176 thermodynamic adsorption/desorption experiments. To this end, 25 mL of aqueous solution at the

177 appropriate pH and ionic strength (NaCl) were placed in the voltammetric cell. A voltammogram of

178 the solution was recorded as blank. Then, voltammograms after addition of different aliquots of the

179 standard solution of Pb^{2+} (100 mgL^{-1}) at the same pH and ionic strength were collected. The

180 concentration range of the calibration curves was 3 - 50 mg L^{-1}.

181 The pH of the Pb^{2+} solutions was measured with a combined ISE-H^{+} glass electrode (Ross type

182 8102). The ISE-H^{+} electrode was previously calibrated at the same experimental conditions of the

183 adsorption experiments. To this end, 25 mL of standardized HCl solution was titrated with NaOH

184 by using a potentiometric titration system (Metrohm, Model 888 Titrando) controlled by the

185 TIAMO software.

186

187 ***2.4. Models for kinetic and isotherm studies of Pb^{2+} adsorption.***

188 Several models have been proposed by different authors to model equilibrium isotherms and

189 kinetics of metal ion adsorption onto several bio-adsorbents.(Park et al., 2010).

190 Here, the pseudo-first order equation of Lagergren (PFO) (eq. 1), the pseudo-second order equation

191 (PSO) (eq. 2) and the intraparticle diffusion equation of Vermeulen (Ver) (eq. 3) were used to fit the

192 kinetic data (Ho, 2006; Park et al., 2010) and references therein:

(1)

$$\frac{dq_t}{dt} = k_1(q_e - q_t)$$

$$\frac{dq_t}{dt} = k_2(q_e - q_t)^2$$

(2)

(3)

$$\frac{dq_t}{dt} = k_v \frac{(q_e^2 - q_t^2)}{q_t}$$

193 where q_t and q_e are the adsorption ability of the adsorbent material (mg g^{-1}) at time t and at the

194 equilibrium and k_1 (min^{-1}), k_2 (g mg^{-1} min) and k_v (min^{-1}) are the rate constants of adsorption.

195 Integrating eqs for the boundary conditions $t = 0$ to $t = t$ and $q_t = 0$ to $q_t = q_t$ in the non linear form

196 are listed below:

$$q_t = q_e(1 - e^{-k_1 t}) \tag{4}$$

$$q_t = \frac{q_e^2 \cdot k_2 \cdot t}{1 + q_e \cdot k_2 \cdot t} \tag{5}$$

$$q_t = q_e \cdot (1 - e^{-2k_v t})^{0.5} \tag{6}$$

197   Batch equilibrium isotherm curves have been obtained processing the experimental data with three

198   empirical models namely the two parameters models of Freundlich (eq. 7) and Langmuir (eq. 8) and

199   the three parameters model of Sips (eq. 9)(Gerente et al., 2007; Park et al., 2010) and references

200   therein:

$$q_e = K_F \cdot C_e^{1/n} \tag{7}$$

$$q_e = \frac{q_m \cdot K_L \cdot C_e}{1 + K_L \cdot C_e} \tag{8}$$

$$q_e = \frac{q_m \cdot K_S \cdot C_e^{1/s}}{1 + K_S \cdot C_e^{1/s}} \tag{9}$$

201   where q_m (mg g^{-1}) is the maximum adsorption capacity of the material, C_e (mg L^{-1}) is the metal

202   concentration in solution at equilibrium; K_F (L$^{1/n}$ g^{-1} mg$^{1-1/n}$), K_L (L·mg^{-1}) and K_S (L$^{1/s}$ mg$^{-1/s}$) are the

203   constants of Freundlich, Langumir and Sips models, respectively. Freundlich model takes into

204   account the heterogeneity of surface or of the binding sites of the adsorbent. K_F and n are related to

205   the binding capacity and the affinity of the adsorbent toward the adsorbate. Langmuir model

206   describes the adsorption on equivalent sites of the material which can be saturated obtaining a

207   monolayer. K_L is related to the initial slope of the isotherm. Finally, in the Sips model both

208   heterogeneous adsorptions as well as saturation conditions are taken into account introducing a third

209   parameter (s) in the equation.

210   The metal ion adsorption capacity at different contact times t (q_t, mg g^{-1}) in kinetic study, or at

211   different metal / adsorbent ratio in equilibrium study (q_e, mg g^{-1}) was calculated by the eq. 10:

$$q_t \ or \ q_e = \frac{V \cdot (C_0 - C_t)}{m} \tag{10}$$

212   where V (L) is the volume of the metal solution and m is the mass of p-Hal or Hal-NH$_2$ (g); C_0 and

213   C_t are the metal ion concentrations in solution (mg L^{-1} of Pb^{2+}) at $t = 0$ and $t = t$, respectively. At the

214   equilibrium condition, eq. 10 was applied by replacing C_t with C_e to calculate q_e.

215   The Linear and Non Linear data Analysis home-made computer program LIANA and OriginLab

216   suite were used to fit kinetic and isotherm equations to experimental data (De Stefano et al., 1997).

217

218   **3. Results and Discussion**

219   **3.1 Synthesis and characterization of Hal-NH$_2$ nanomaterial**

220   Halloysite nanotubes reacted with an excess of 3-azidopropyltrimethoxysilane in toluene at reflux,

221   affording the Hal-N$_3$ nanomaterial, following a procedure reported elsewhere (Riela et al., 2014).

222   After the work up, the -N$_3$ groups loading with respect to p-Hal, estimated by TGA, was ca. 2.4 $\pm$

223   0.2 wt%. Successively, the quantitative reduction with PPh$_3$ of Hal-N$_3$, gave amino-functionalized

224   Hal-NH$_2$ that represents the adsorbent material (see Figure 1).

225   To confirm that the functionalization occurs on the external surface, contact angle measurements

226   were performed obtaining the θ values of 21.9 $\pm$ 1.3° and 61.2 $\pm$ 1.3°, for p-Hal and Hal-NH$_2$,

227   respectively.

228

229
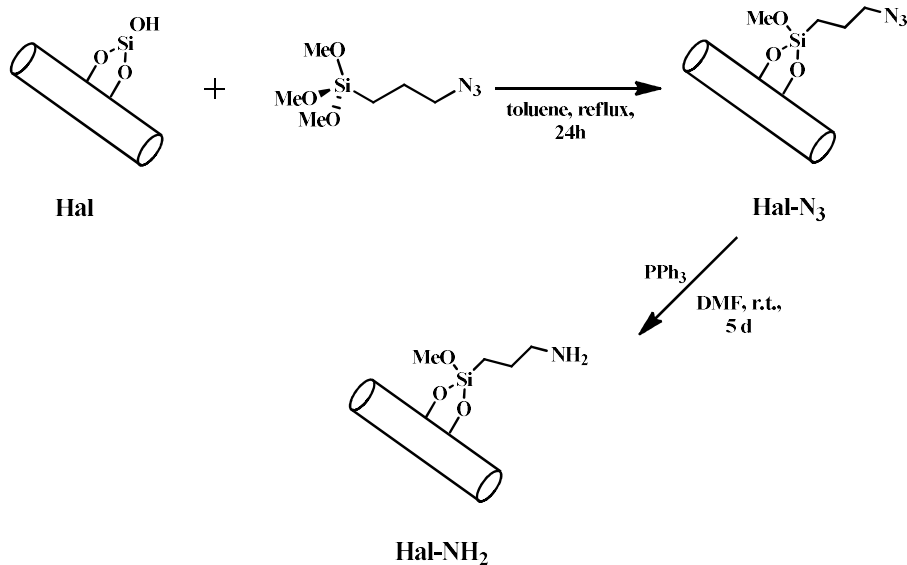
Figure 1. Schematic representation of the synthesis of Hal-NH$_2$ nanomaterial.

The two-step synthesis was adopted in order to ensure the highest loading on halloysite external surface; for comparison, indeed, we also performed a one-step modification with 3-aminopropyltrimethoxysilane, which gave a percent loading of about 1 wt% whereas the introduction of the azido group and the following reduction allowed us to obtain a loading of 2.4 wt%.

Compared to p-Hal, (Massaro et al., 2016a) Hal-N$_3$ nanomaterial exhibits the vibration bands for C–H stretching of methylene groups around 2980 cm^{-1} and a strong band around 2100 cm^{-1} due to the –N$_3$ groups of azido silane. The intensity for -N$_3$ band decreases after reduction confirming the presence of the NH$_2$ groups on halloysite external surface. These findings provide evidence for the presence of organic moieties in the new material (Figure 2a). Based on the unaltered frequency of the stretching bands of OH groups of the alumina inner-surface, we can conclude that the grafting has taken place only on the external surface of Hal, as reported elsewhere (Rawtani et al., 2017; Sadjadi and Atai, 2018).

Thermogravimetric analyses (TGA) confirmed the functionalization on p-Hal external surface and it allowed calculating 2.4 wt% loading of organic moiety on the Hal-NH$_2$ nanomaterial as follow:

248

$$wt\% = 100[1 - (MR_{600\text{-Hal-NH}_2} + ML_{150\text{-Hal-NH}_2})/(MR_{600\text{-p-Hal}} + ML_{150\text{-p-Hal}})] \quad (11)$$

249

250 where $MR_{600\text{-Hal-NH}_2}$ and $MR_{600\text{-p-Hal}}$ are the residual mass at 600 °C obtained from TG curves of

251 amine functionalized halloysite and pristine halloysite, respectively, while ML_{150} is the mass loss

252 between 25 and 150 °C representing the water content of the investigated material.

253 The curves (Figure 2b) clearly show that the residual of the nanomaterials is stepwise changing,

254 from the p-Hal to the Hal-NH$_2$, due to the organic compounds linked on the surface of the

255 nanotubes. The thermograms were corrected for the different moisture contents to underline the

256 mass losses of p-Hal and organic compounds. Above 100 °C the p-Hal curve reveals the

257 characteristic mass loss at 500 °C attributed to the expulsion of two water molecules from p-Hal

258 interlayer (Massaro et al., 2016b). The Hal-NH$_2$, instead, showed an additional mass loss at 250 °C

259 due to the organic moiety with NH$_2$ termination (Cavallaro et al., 2015).

260

(2a)

(2b)
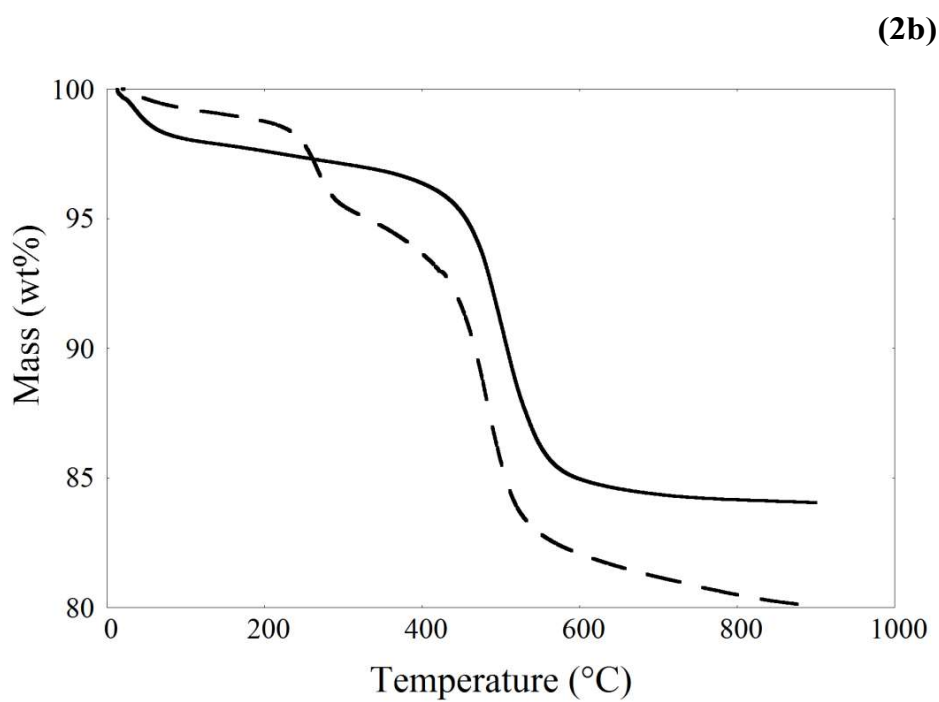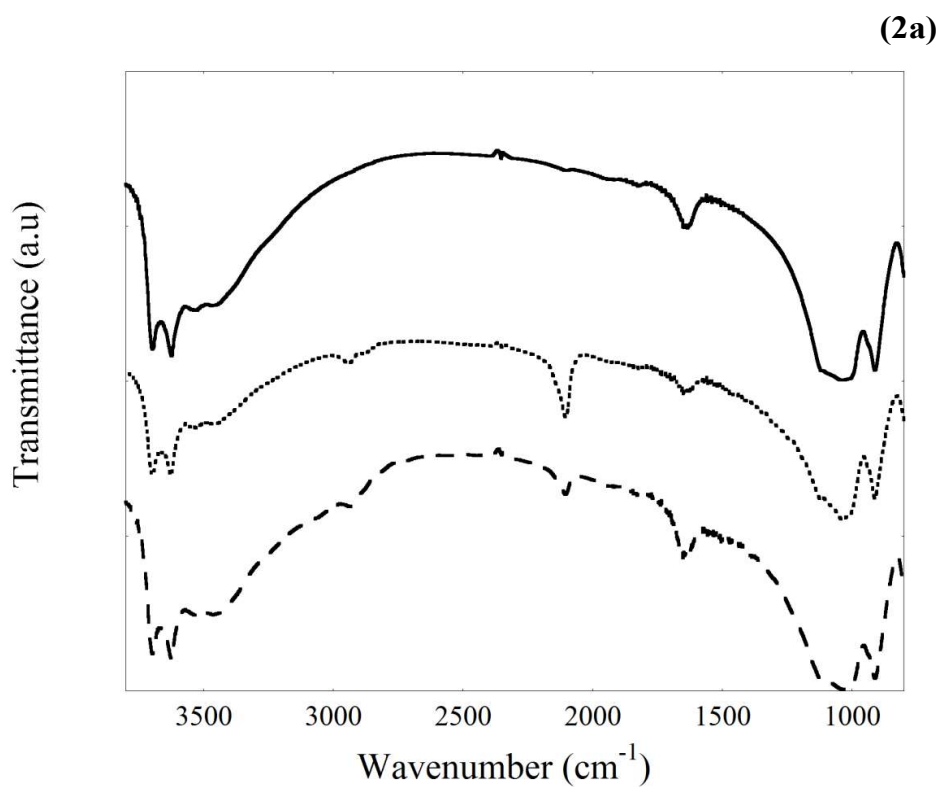
Figure 2. FT-IR spectra of p-Hal (solid line), Hal-N$_3$ (dotted line) and Hal-NH$_2$ (dashed line) (2a); thermoanalytical curves of p-Hal (solid line) and Hal-NH$_2$ (dashed line) (2b).

The morphology of functionalized Hal was characterized by electron scanning microscopy (SEM) (see Figure 3). SEM image shows that in the Hal-NH$_2$ compound the morphology of Hal was preserved after organosilane grafting and the nanomaterial shows the typical rod-shaped structure of halloysite.
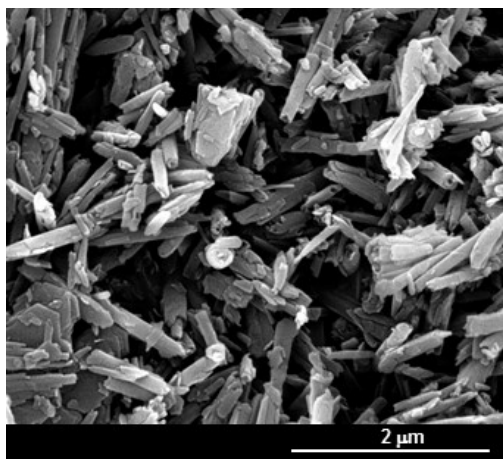
Figure 3. SEM image of Hal-NH$_2$.

3.2 Speciation Analysis

An efficient metal ion adsorption onto an adsorbent mainly depends on the chemical form of the adsorbent and adsorbate in the aqueous solution to be treated.

In particular, the metal ion has to be present in solution as positively or negatively charged species able to interact with binding groups with opposite charge on the adsorbent.

The chemical form of metal ion, as well as that of the adsorbent material depends on the experimental conditions of the aqueous solution (ionic medium, ionic strength, pH, etc.) and only an accurate speciation study gives the possibility to know the best conditions in terms of adsorption ability of the adsorbent towards the toxic metal ion.

As it is known, the inner and outer surfaces of halloysite nanotubes contain AlOH and SiOH groups, respectively. Due to their acid-base properties, in a wide pH range there is a charge separation between the external (negative) and internal (positive) surfaces of the nanotubes. In

283 addition, in the functionalized halloysite Hal-NH$_2$ also the propylamine groups bound to the outer

284 surface have to be considered.

285 The protonation equilibria of p-Hal have been studied in a previous article in different ionic media

286 and ionic strengths (Bretti et al., 2016). Two units namely p-Hal$_1$ and p-Hal$_2$ containing AlOH and

287 SiOH groups, respectively were considered to model the protonation equilibria of halloysite.

288 Different models, previously tested for natural and synthetic polyelectrolytes, were used to calculate

289 protonation constants. Here, the protonation constants calculated with diprotic like model have been

290 used to draw the distribution diagrams of protonated/unprotonated p-Hal species in NaCl medium

291 chosen in adsorption experiments. As an example, Figure 1S of Supplementary Materials reports

292 the distribution diagram of p-Hal$_1$ and p-Hal$_2$ species in NaCl$_{aq}$, at $I = 0.1$ mol L^{-1} and $T = 25$ °C.

293 In the ionic medium and pH range considered, Pb^{2+} ion forms several hydroxo and chloride species

294 differently charged [Pb(OH)$_n^z$, PbCl$_n^z$ and PbCl(OH) n = 0 to 3, z = from 2+ to 1-]. Also the

295 formation and distribution of metal species have been evaluated using the stability constants in

296 NaCl medium reported in the literature (Baes and Mesmer, 1976; Luo and Millero, 2007). As an

297 example, the speciation diagram of Pb^{2+} species in NaCl aqueous solution at $I = 0.1$ mol L^{-1} is

298 reported in Figure 2S of Supplementary materials.

299 Table 1 reports the percentages of p-Hal and Pb^{2+} species as function of pH and ionic strength in

300 NaCl medium and at $T = 25$ °C. These data, and those at lower and higher pH values (not reported

301 here) have been taken into account to establish the best experimental conditions used in adsorption

302 experiments and they are discussed in section 3.4.

303

304

305 **Table 1.** Percentages of Pb(II) and p-Hal species[a] in NaCl aqueous solution, at different ionic

306 strengths and pH and at $T = 25$ °C

species	%

pH	3	4	5	5	5	6
I (mol L^{-1})	0.10	0.10	0.10	0.25	0.50	0.10
p-Hal$_1$	0	0	0	0	0	0
H(p-Hal$_1$)$^+$	0	0.01	0.1	0.11	0.09	0.97
H$_2$(p-Hal$_1$)$^{2+}$	100	99.99	99.9	99.89	99.81	99.03
pHal$_2^-$	6	38.96	86.45	84.18	82.55	98.46
H(p-Hal$_2$)	94	61.04	13.55	15.82	17.45	1.54
Pb^{2+}	24.5	24.5	24.3	11.7	5.8	22.8
PbCl$^+$	56.0	56.0	55.6	48.6	36.5	52.3
PbCl$_2$	18.5	18.5	18.4	35.0	46.0	17.3
PbCl$_3^-$	1.0	1.0	1.0	4.4	11.5	0.9
Pb(OH)$^+$	0	0.1	0.7	0.3	0.2	6.6
PbCl(OH)	0	0	0	0	0	0.1

307 [a] calculated from distribution diagrams made by using the formation constants of p-Hal and Pb(II)

308 species reported in ref. (Baes and Mesmer, 1976; Luo and Millero, 2007; Bretti et al., 2016) and the

309 same concentrations used in the adsorption experiments.

310

311 **3.3 Kinetics of Pb(II) adsorption on p-Hal and Hal-NH$_2$ materials**

312

313 The Pb^{2+} adsorption rate onto p-Hal and Hal-NH$_2$ has been studied in NaCl aqueous solution at $I =$

314 0.1 mol L^{-1}, $C_{Pb^{2+}} = 30$ mg L^{-1}, in the pH range 3 - 6. Independently of pH, the adsorption

315 equilibrium in Pb^{2+}- p-Hal system was reached very quickly (~ 40 min). The same behaviour was

316 found with Hal-NH$_2$ at pH = 3, whilst at higher pH, after an initial rapid Pb^{2+} adsorption (~ 40 min),

317 there was a slow and continue adsorption until ~ 240 min (see Figures 3S and 4S).

318   In order to understand the adsorption dynamics, different kinetic models were used to fit

319   experimental data (see section 2.4). The values of kinetic parameters of PFO, PSO and Ver models

320   are reported in Table 2S together with R^2 and σ of the fits. The most suitable kinetic model for Pb^{2+}

321   -p-Hal system at every pH and for Pb^{2+} - Hal-NH_2 system at pH = 3 was the PFO, whilst, at higher

322   pH the Ver model better described the experimental data of Pb^{2+} - Hal-NH_2 system (see Table 2). It

323   can be explained considering that at pH = 3 the great part of binding groups of both adsorbents are

324   protonated, their adsorption capacity is low and their behaviour is very similar. At higher pH the

325   deprotonation of SiOH groups of halloysite favours the adsorption of both adsorbents; moreover

326   also amino groups contribute to the Pb^{2+} adsorption of Hal-NH_2 increasing its adsorption ability

327   (e.g. q_e = 4.30 and 18.6 mg g^{-1} at pH = 5 for p-Hal and Hal-NH_2, respectively) and changing the

328   adsorption dynamics of the functionalized p-Hal (Ver model fit better than PFO model; see R^2 and

329   σ values in Table 2S). The q_e trends of the two adsorbents *vs* pH are shown in Figure 5S of

330   Supplementary Materials.

331

332   **Table 2.** Parameters of PFO and Ver kinetic equations for Pb(II) adsorption on p-Hal and Hal-NH_2,

333   at different pH values, in NaCl$_{aq}$, at I = 0.1 mol L^{-1} and at T = 25 °C.

Kinetic model	adsorbent	pH	q_e[a]	k_i[b,c]	R^2	σ[d]
PFO	p-Hal	3	3.00 ± 0.01	0.154 ± 0.005	0.9848	0.0849
PFO	Hal-NH_2		3.74 ± 0.02	0.187 ± 0.009	0.9715	0.1417
PFO	p-Hal	4	3.27 ± 0.02	0.139 ± 0.005	0.9856	0.0940
Ver	Hal-NH_2		13.1 ± 0.4	0.003 ± 0.001	0.9888	0.3831
PFO	p-Hal	5	4.30 ± 0.03	0.21 ± 0.01	0.9749	0.1413
Ver	Hal-NH_2		18.6 ± 0.4	0.0034 ± 0.0001	0.9902	0.4934
PFO	p-Hal	6	5.03 ± 0.05	0.101 ± 0.006	0.9576	0.2654
Ver	Hal-NH_2		19.7 ± 0.7	0.0022 ± 0.0002	0.9880	0.5651

334   [a] mg g^{-1}; [b] min^{-1} for both k_1 and k_v; [c] subscript i is 1 or v according to the model; [d] std. dev of the fit.

335

3.4 Modelling of equilibria of Pb(II) uptake by p-Hal and Hal-NH$_2$ materials

Adsorption equilibria of Pb^{2+} onto p-Hal and Hal-NH$_2$ have been studied in NaCl aqueous solutions in the pH range 3 – 6 chosen on the basis of speciation analysis (see section 3.2). The solution pH was measured at the end of experiments and is reported in Table 3 together with parameters of the most suitable isotherm equation for each experimental data set. Among the tested isotherm models, Sips equation was the best or it was equivalent to Langmuir isotherm ($s \approx 1$) in terms of quality of fit for all the systems investigated. Although isotherm models do not necessarily give information about the mechanism of the adsorption of metal ion they can be useful to predict or optimize the uptake processes, e.g., through the calculation of q_m parameter that gives information about the maximum amount of metal ion adsorbed by 1 g of adsorbent. The parameters of all isotherm equations tested are reported in Table 3S of Supplementary Materials together with the R^2 and σ of the fits. In batch experiments, a significant increase of pH of solutions (1.5 – 2 units) at the adsorption equilibrium was found only with Hal-NH$_2$ adsorbent at initial pH = 4, 5 and 6 and can be attributed to the protonation of amino groups not bound to Pb^{2+} ions. In fact, considering the concentration of Pb^{2+} and the amount of adsorbent used in batch experiments, NH$_2$ groups of adsorbent are always in excess with respect to the metal ion.

The experimental points together with the curve fits of the three isotherm equations for all the Pb(II) – adsorbent investigated systems are reported in Figure 4 and in Figures 6S and 7S of Supplementary Materials. The adsorption ability of both pristine and functionalized Hal increases with the increasing of pH and with the decreasing of ionic strength (see Figures 5 and 6). Looking at the species percentages reported in Table 1, in the pH and ionic strength ranges investigated the great part of Pb(II) is present as positively charged species [Pb^{2+}, PbCl$^+$ and Pb(OH)$^+$] easily bounded by silanol and amino groups of adsorbent materials. Moreover, at $I = 0.1$ mol L^{-1} the % of Pb species, as well as the % of p-Hal$_1$ species do not change with the changing of pH from 3 to 6. Therefore, the increase of q_m with pH for both p-Hal and Hal-NH$_2$ can be ascribed to the

18

deprotonation of SiOH groups of p-Hal$_2$ units (Bretti et al., 2016) of halloysite (% p-Hal$_2^-$ = 6 and 98 at pH 3 and 6, respectively) and to the presence of NH$_2$ groups in Hal-NH$_2$ material that are fully protonated at pH = 3 and becomes gradually available to bind Pb^{2+} ions at higher pH values. At pH = 5, the increase of ionic strength from 0.1 to 0.5 mol L^{-1} causes a decrease of positively charged Pb species (substituted by chlorinated PbCl$_2$ and PbCl$_3^-$ species) that is responsible of the lowering of q_m of p-Hal and of Hal-NH$_2$.

Independently of the experimental conditions, the adsorption ability, as well as the affinity of Hal-NH$_2$ towards Pb^{2+} are higher than p-Hal (higher q_m and K_s values) and the differences in adsorptive performances of the two materials are more pronounced at higher pH values (e.g., q_m = 6 and 46 mg g^{-1}, K_s = 0.017 and 0.43 L$^{1/s}$ mg$^{-1/s}$ at pH = 6 for p-Hal and Hal-NH$_2$, respectively).

Considering i) the changing of pH during adsorption, ii) the speciation analysis of p-Hal and of Pb^{2+} ion in aqueous solution and iii) the dependence on pH and ionic strength of adsorption ability of p-Hal and Hal-NH$_2$, an adsorption mechanism mainly based on positively charged Pb^{2+} species [Pb^{2+}, Pb(OH)$^+$ and PbCl$^+$] chelation by silanol and amino groups can be hypothesized.

Table 3. Sips isotherm parameters for the Pb(II) adsorption on p-Hal and Hal-NH$_2$ in NaCl$_{aq}$, at different pH and ionic strengths and at T = 25 °C.

adsorbent	pH$_i$[a]	pH$_f$[a]	I[b]	q_m[c]	K_s[d]	s	R^2	σ[e]
p-Hal	3.0±0.2	3.1±0.2	0.10	3.10±0.03	0.016±0.003	0.80±0.06	0.9974	0.0469
Hal-NH$_2$	2.9±0.3	3.1±0.4		5±1	0.010±0.004	0.7±0.1	0.9848	0.1420
p-Hal	4.0±0.3	4.0±0.3	0.10	3.5±0.4	0.013±0.001	0.84±0.06	0.9982	0.0282
Hal-NH$_2$	4.0±0.3	6.0±0.2		19.1±0.4	0.57±0.04	1.00±0.01	0.9979	0.2627
p-Hal	5.0±0.2	5.3±0.3	0.10	4.5±0.2	0.03±0.01	0.66±0.08	0.9907	0.1378
Hal-NH$_2$	5.0±0.2	6.7±0.6		37±2	0.69±0.08	2.1±0.2	0.9978	0.4640

p-Hal	5.0±0.2	5.2±0.3	0.25	3.3±0.6	0.037±0.009	0.9±0.2	0.9847	0.1013
Hal-NH$_2$	5.0±0.2	6.3±0.5		31±2	0.41±0.5	1.6±0.2	0.9926	0.7261
p-Hal	5.0±0.2	5.2±0.2	0.50	1.40±0.04	0.009±0.003	0.50±0.04	0.9944	0.0365
Hal-NH$_2$	5.0±0.2	6.2±0.5		28±6	0.31±0.7	1.6±0.4	0.9791	1.0020
p-Hal	6.0±0.2	6.1±0.2	0.10	6±1	0.017±0.002	0.98±0.08	0.9972	0.0474
Hal-NH$_2$	6.0±0.2	6.8±0.4		46±7	0.43±0.09	2.1±0.3	0.9943	0.7821

379 [a] solutions pH before (pH$_i$) and after (pH$_f$) contact with adsorbents; [b] mol L^{-1}; [c] mg g^{-1}; [d] L$^{1/s}$ mg$^{-1/s}$; [e]

380 std. dev of the fit.

381
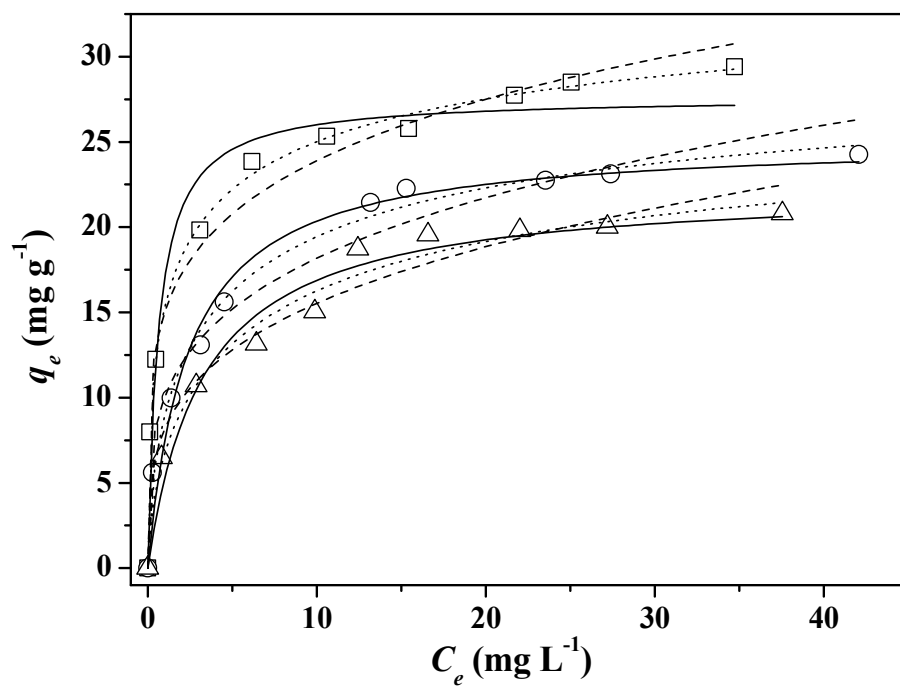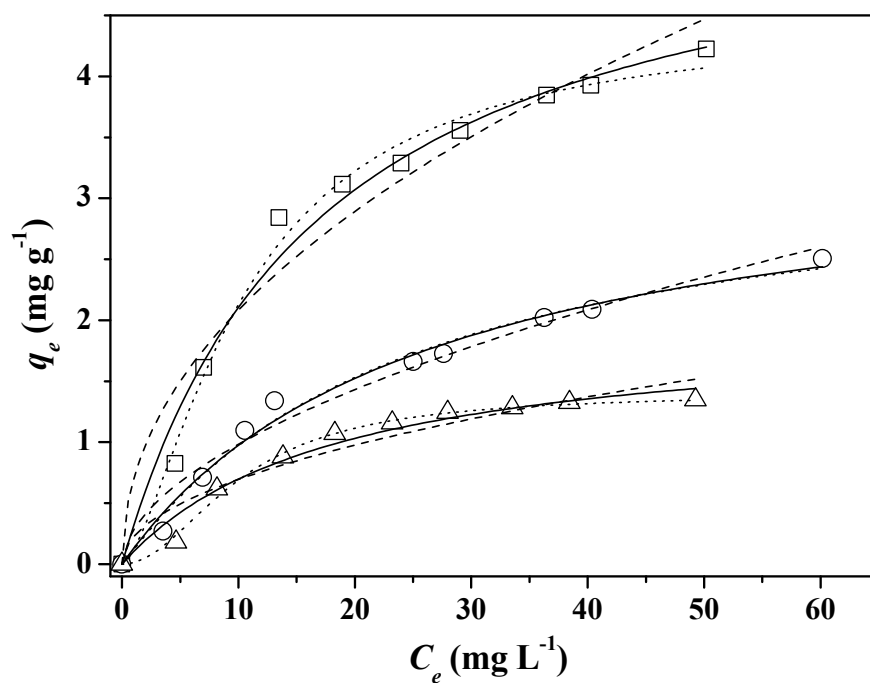
382 **Figure 4.** Adsorption isotherms of Pb^{2+} on Hal-NH$_2$ (Fig. 3a) and p-Hal (Fig. 3b) from aqueous

383 solutions at pH = 5 containing NaCl 0.10 ($\square$), 0.25 ($\bigcirc$), 0.50 ($\triangle$) mol L^{-1} and at T = 25 °C.

384   Experimental data fitted with Freundlich (dashed lines), Langmuir (continuous lines) and Sips

385   (dotted lines) models.
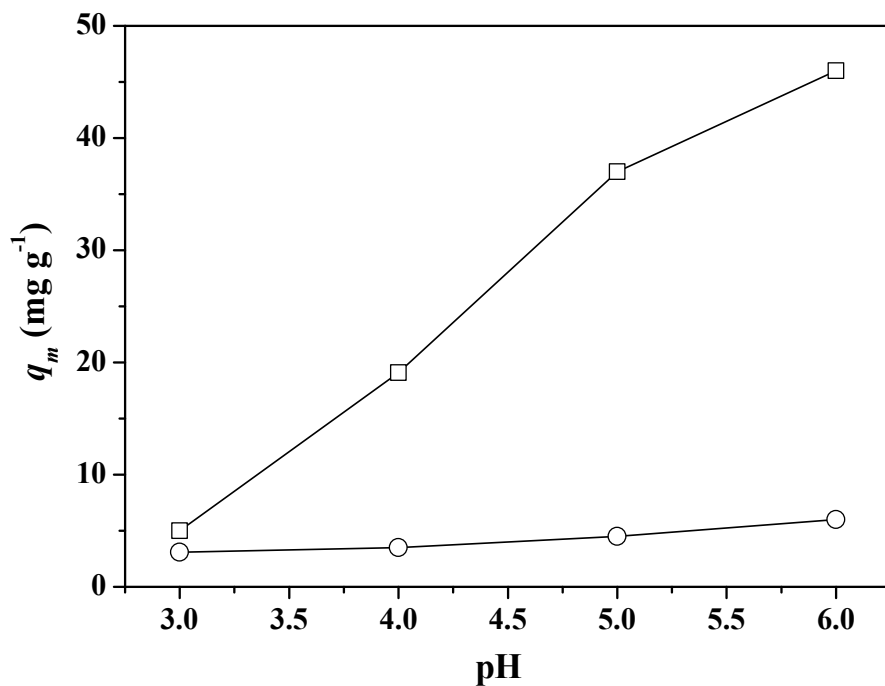
386

387   **Figure 5.** Experimental q_m values *vs* pH for the Pb^{2+} adsorption onto p-Hal ($\bigcirc$) and Hal-NH$_2$ ($\square$)

388   adsorbent materials in NaCl$_{aq}$, at $I = 0.10$ mol L^{-1} and $T = 25$ °C.

389
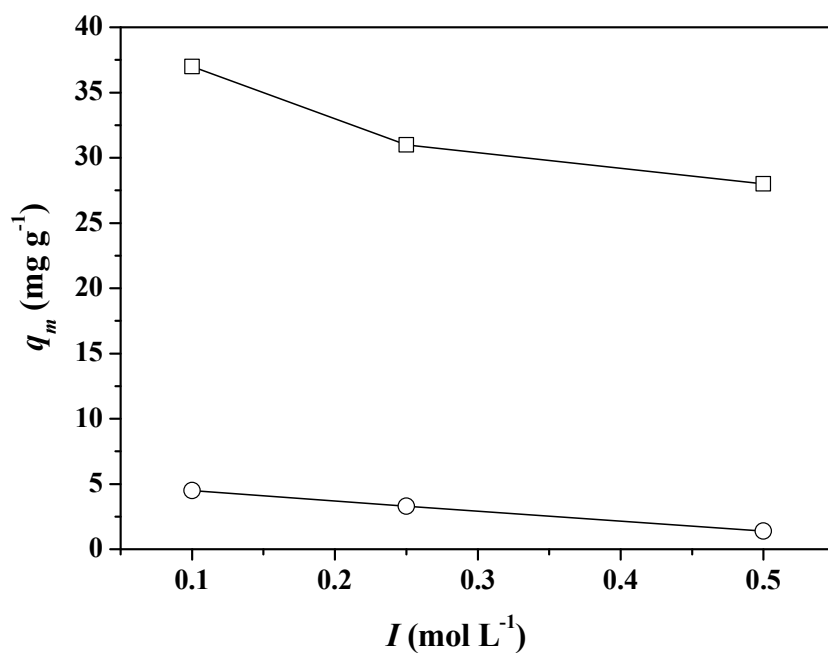
Figure 6. Experimental q_m values *vs* I (mol L^{-1}) for the Pb^{2+} adsorption onto p-Hal ($\bigcirc$) and Hal-NH_2 ($\square$) adsorbent materials in $NaCl_{aq}$, at pH = 5 and $T = 25$ °C.

The possibility of recycle and reuse of Hal-NH_2 material has been evaluated. The results of adsorption/desorption cycles are shown in Figure 7. As can be seen, at the conditions used in the experiments, the adsorbent exhibits a good reuse capacity with slight variations of adsorbed/desorbed amount of Pb^{2+} in the first three cycles.

400
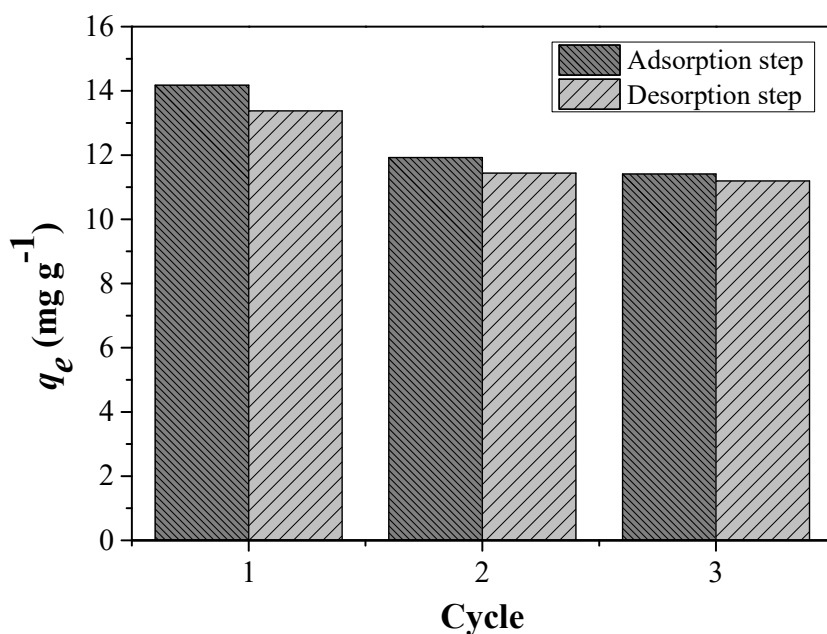
Figure 7. q_e values of adsorption and desorption steps. Experimental details: amount of Hal-NH$_2$ =

40 mg, $C_{Pb^{2+}}$ = 30 mg L^{-1} in NaCl, at I = 0.1 mol L^{-1}.

3.5 Literature data comparison

In the last decades a lot of articles and reviews have been published on the adsorption ability of

different pristine or modified clay minerals towards Pb^{2+} ions (Jiang et al., 2009; Oubagaranadin

and Murthy, 2009; He et al., 2013; Matusik and Wscislo, 2014; Maziarz et al., 2015; Yuan et al.,

2015; Sdiri et al., 2016; Hu et al., 2017; Uddin, 2017). A comparison of the adsorption capacity of

the different clay adsorbents is very difficult because it depends on many variables of the metal –

adsorbent system investigated such as: the origin of the clay, the type of modification, the loading

percent (in case of functionalization), the experimental conditions of metal ion solution (pH, ionic

medium, ionic strength, metal ion concentration, temperature). In Table 4 are reported the ranges of

maximum adsorption capacity values (q_m) of different pristine and modified clay minerals towards

Pb^{2+} recently reported in literature. On average, the adsorption ability of p-Hal toward Pb^{2+} is lower

than other clay minerals. However, p-Hal has a good dispersability in water and does not need

exfoliation to expose large surface area in an efficient way.

Considering the experimental differences, the adsorption results here obtained for p-Hal towards

Pb^{2+} ion are comparable with those reported in literature by (Matusik and Wscislo, 2014) and

(Maziarz et al., 2015). The authors reported a q_m = 8 and 7.7 mg g^{-1}, respectively, at pH = 5 and

without ionic medium. Considering the absence of Pb-Cl species and the consequently higher

percent of positively charged Pb species in solution, these q_m values are in line with the q_m = 4.5 mg

g^{-1} that we found at the same pH, in NaCl$_{aq}$ at I = 0.1 mol L^{-1}. Two functionalized Hal with

diethanolamine (HD) and triethanolamine (HT) were also tested as adsorbent materials towards

Pb^{2+} ion by (Matusik and Wscislo, 2014). The q_m = 37 mg g^{-1} found by us for Hal-NH$_2$ at pH = 5

and I = 0.1 mol L^{-1} is significantly higher than 13.28 and 12.18 mg g^{-1} found at the same pH and

without chloride medium for HD and HT, respectively. These differences in q_m values could be

attributed to the steric indrance produced by the two or three ethanol groups of HD and HT that

hampered the Pb^{2+} interaction with amino groups of the functionalized Hal. Moreover, the

functionalization of Hal in HD and HT adsorbents occurs in the interlayers of Hal.

Table 4. Literature maximum adsorption capacity values (q$_m$) of different clay minerals

p or m clay[a]	q_m[b]	ref
p-kaol[c]	0.12–11.50	(Jiang et al., 2009; Oubagaranadin and Murthy, 2009; Uddin, 2017)
m-Kaol	25.13–82.65	(Jiang et al., 2009; Uddin, 2017)
p-Mont	31.10–37.16	(Sdiri et al., 2016; Uddin, 2017)
m-Mont	71.92-121.95	(Hu et al., 2017; Uddin, 2017)
p-Smec	3.13 – 75.35	(Uddin, 2017)
p-Sep	30.5	(Sdiri et al., 2016)
p-Bent	28.00 - 51.19	(Sdiri et al., 2016; Uddin, 2017)

m-Bent	110	(Uddin, 2017)
p-Pal	62.1	(Oubagaranadin and Murthy, 2009)
p-Hal	6 - 8	(Matusik and Wscislo, 2014; Maziarz et al., 2015), this work
m-Hal	12.18 - 46	(He et al., 2013; Matusik and Wscislo, 2014), this work

432   [a] p = pristine, m = modified; [b] $mg\ g^{-1}$; c Kaol = Kaolinite; Mont = Montmorillonite; Smec =

433   Smectite; Sep = Sepiolite, Bent = Bentonite, Pal = Palygorskite.

434

435   **4. Conclusions**

436   Functionalized halloysite nanotubes with amino groups (Hal-NH_2) have been successfully

437   employed as adsorbent for Pb^{2+} ions. Their adsorption ability was kinetically and

438   thermodynamically studied. Results were compared with that of p-Hal in NaCl aqueous solutions

439   and in the pH range 3 -6. The best experimental conditions for the metal ion removal were

440   established on the basis of a speciation study of Pb^{2+} and of the p-Hal. The results obtained can be

441   summarized as follows:

442   1.   FT-IR, TGA and contact angle analysis on Hal-NH_2 material confirm the successful outcome

443   of synthesis with a 2.4 wt% loading of organic moiety on the nanomaterial, whilst, the

444   preservation of morphology of p-Hal after organosilane grafting was showed by SEM

445   analysis;

446   2.   several kinetic and isotherm equations were used to fit experimental data and the parameters

447   of the most suitable models were analyzed to discuss the adsorption performances of the two

448   adsorbent materials;

449   3.   an improvement of the adsorption ability of both pristine and functionalized p-Hal materials

450   was found with the increasing of pH and the decreasing of ionic strength;

451   4.   the adsorption ability of amino-functionalized Hal-NH_2 towards Pb^{2+} is considerable higher

452   than that of p-Hal and of other functionalized halloysite reported in literature.

453   5.   The Hal-NH$_2$ shows a noticeable reuse capability that encourages the use of this material as

454   adsorbent of Pb^{2+} ions in the pH and ionic strength ranges considered.

455

456   **Acknowledgements**

459

460

References

Baes, C.F., Mesmer, R.E., 1976. The Hydrolysis of Cations. John Wyley & Sons, New York.

Bretti, C., Cataldo, S., Gianguzza, A., Lando, G., Lazzara, G., Pettignano, A., Sammartano, S., 2016. Thermodynamics of Proton Binding of Halloysite Nanotubes. J. Phys. Chem. C 120, 7849-7859.

Cataldo, S., Muratore, N., Orecchio, S., Pettignano, A., 2015. Enhancement of adsorption ability of calcium alginate gel beads towards Pd(II) ion. A kinetic and equilibrium study on hybrid Laponite and Montmorillonite-alginate gel beads. Appl. Clay Sci. 118, 162-170.

Cavallaro, G., Lazzara, G., Massaro, M., Milioto, S., Noto, R., Parisi, F., Riela, S., 2015. Biocompatible Poly(N-isopropylacrylamide)-halloysite Nanotubes for Thermoresponsive Curcumin Release. J. Phys. Chem. C 119, 8944-8951.

Cavallaro, G., Lazzara, G., Milioto, S., Parisi, F., Sanzillo, V., 2014. Modified Halloysite Nanotubes: Nanoarchitectures for Enhancing the Capture of Oils from Vapor and Liquid Phases. ACS Appl. Mater. Inter. 6, 606-612.

De Stefano, C., Sammartano, S., Mineo, P., Rigano, C., 1997. Computer Tools for the Speciation of Natural Fluids, in: Gianguzza, A., Pelizzetti, E., Sammartano, S. (Eds.), Marine Chemistry - An Environmental Analytical Chemistry Approach. Kluwer Academic Publishers, Amsterdam, pp. 71-83.

Dong, Y., Liu, Z., Chen, L., 2012. Removal of Zn(II) from aqueous solution by natural halloysite nanotubes. J. Radioanal. Nucl. Chem. 292, 435-443.

Fan, L., Zhang, J., Wang, A., 2013. In situ generation of sodium alginate/hydroxyapatite/halloysite nanotubes nanocomposite hydrogel beads as drug-controlled release matrices. J. Mater. Chem. B 1, 6261-6270.

Förstner, U., Salomons, W., Mader, P., eds., 1995. Heavy Metals, Problems and Solutions. Springer-Verlag Berlin Heidelberg.

Gerente, C., Lee, V.K.C., Cloirec, P.L., McKay, G., 2007. Application of Chitosan for the Removal of Metals From Wastewaters by Adsorption-Mechanisms and Models Review. Crit. Rev. Env. Sci. Technol. 37, 41-127.

Gidlow, D.A., 2015. Lead toxicity. Occupational Medicine 65, 348-356.

He, Q., Yang, D., Deng, X., Wu, Q., Li, R., Zhai, Y., Zhang, L., 2013. Preparation, characterization and application of N-2-Pyridylsuccinamic acid-functionalized halloysite nanotubes for solid-phase extraction of Pb(II). Water Research 47, 3976-3983.

Hebbar, R.S., Isloor, A.M., Ananda, K., Ismail, A.F., 2016. Fabrication of polydopamine functionalized halloysite nanotube/polyetherimide membranes for heavy metal removal. J. Mater. Chem. A 4, 764-774.

Ho, Y.-S., 2006. Review of second-order models for adsorption systems. J. Hazard. Mater. 136, 681-689.

Hu, C., Zhu, P., Cai, M., Hu, H., Fu, Q., 2017. Comparative adsorption of Pb(II), Cu(II) and Cd(II) on chitosan saturated montmorillonite: Kinetic, thermodynamic and equilibrium studies. Appl. Clay Sci. 143, 320-326.

Jiang, M.-q., Wang, Q.-p., Jin, X.-y., Chen, Z.-l., 2009. Removal of Pb(II) from aqueous solution using modified and unmodified kaolinite clay. J. Hazard. Mater. 170, 332-339.

Jinhua, W., Xiang, Z., Bing, Z., Yafei, Z., Rui, Z., Jindun, L., Rongfeng, C., 2010. Rapid adsorption of Cr (VI) on modified halloysite nanotubes. Desalination 259, 22-28.

Joussein, E., Petit, S., Churchman, J., Theng, B., Righi, D., Delvaux, B., 2005. Halloysite clay minerals - a review. Clay Miner. 40, 383-426.

Kurczewska, J., Grzesiak, P., Lukaszyk, J., Gabala, E., Schroeder, G., 2015. High decrease in soil metal bioavailability by metal immobilization with halloysite clay. Environ. Chem. Lett. 13, 319-325.

510 Liu, M., Chang, Y., Yang, J., You, Y., He, R., Chen, T., Zhou, C., 2016. Functionalized halloysite
511 nanotube by chitosan grafting for drug delivery of curcumin to achieve enhanced anticancer
512 efficacy. J. Mater. Chem. B 4, 2253-2263.
513 Liu, M., Jia, Z., Liu, F., Jia, D., Guo, B., 2010. Tailoring the wettability of polypropylene surfaces
514 with halloysite nanotubes. J. Colloid Interf. Sci. 350, 186-193.
515 Luo, Y., Millero, F.J., 2007. Stability constants for the formation of lead chloride complexes as a
516 function of temperature and ionic strength. Geochim. Cosmochim. Ac. 71, 326-334.
517 Lvov, Y., Wang, W., Zhang, L., Fakhrullin, R., 2015. Halloysite Clay Nanotubes for Loading and
518 Sustained Release of Functional Compounds. Advanced Materials 28, 1227-1250.
519 Lvov, Y.M., DeVilliers, M.M., Fakhrullin, R.F., 2016. The application of halloysite tubule nanoclay
520 in drug delivery. Expert Opinion on Drug Delivery 13, 977-986.
521 Mason, L.H., Harp, J.P., Han, D.Y., 2014. Pb Neurotoxicity: Neuropsychological Effects of Lead
522 Toxicity. BioMed Res. Int. 2014, 8.
523 Massaro, M., Colletti, C.G., Lazzara, G., Guernelli, S., Noto, R., Riela, S., 2017. Synthesis and
524 Characterization of Halloysite - Cyclodextrin Nanosponges for Enhanced Dyes Adsorption. ACS
525 Sust. Chem. Eng. 5, 3346 - 3352.
526 Massaro, M., Riela, S., Baiamonte, C., Blanco, J.L.J., Giordano, C., Lo Meo, P., Milioto, S., Noto,
527 R., Parisi, F., Pizzolanti, G., Lazzara, G., 2016a. Dual drug-loaded halloysite hybrid-based
528 glycocluster for sustained release of hydrophobic molecules. RSC Advances 6, 87935-87944.
529 Massaro, M., Schembri, V., Campisciano, V., Cavallaro, G., Lazzara, G., Milioto, S., Noto, R.,
530 Parisi, F., Riela, S., 2016b. Design of PNIPAAM covalently grafted on halloysite nanotubes as a
531 support for metal-based catalysts. RSC Advances 6, 55312-55318.
532 Matusik, J., 2014. Arsenate, orthophosphate, sulfate, and nitrate sorption equilibria and kinetics for
533 halloysite and kaolinites with an induced positive charge. Chemical Engineering Journal 246, 244-
534 253.
535 Matusik, J., 2016. Halloysite for Adsorption and Pollution Remediation, in: Yuan, P., Thill, A.,
536 Bergaya, F. (Eds.), Nanosized Tubular Clay Minerals - Halloysite and Imogolite Elsevier, pp. 606-
537 627.
538 Matusik, J., Wscislo, A., 2014. Enhanced heavy metal adsorption on functionalized nanotubular
539 halloysite interlayer grafted with aminoalcohols. Appl. Clay Sci. 100, 50-59.
540 Maziarz, P., Prokop, A., Matusik, J., 2015. A comparative study on the removal of Pb(II), Zn(II),
541 Cd(II) and As(V) by natural, acid activated and calcinated halloysite. Geol. Geophys. Env. 41, 108-
542 109.
543 Meng, Q., Chen, H., Lin, J., Lin, Z., Sun, J., 2016. Zeolite A synthesized from alkaline assisted pre-
544 activated halloysite for efficient heavy metal removal in polluted river water and industrial
545 wastewater. J. Environ. Sci., in press.
546 Oubagaranadin, J.U.K., Murthy, Z.V.P., 2009. Adsorption of Divalent Lead on a Montmorillonite -
547 Illite Type of Clay. Ind. Eng. Chem. Res. 48, 10627-10636.
548 Park, D., Yun, Y.-S., Park, J.M., 2010. The past, present, and future trends of biosorption.
549 Biotechnol. Bioproc. E. 15, 86-102.
550 Peng, Q., Liu, M., Zheng, J., Zhou, C., 2015. Adsorption of dyes in aqueous solutions by chitosan -
551 halloysite nanotubes composite hydrogel beads. Micropor. Mesopor. Mat. 201, 190-201.
552 Rawtani, D., Pandey, G., Tharmavaram, M., Pathak, P., Akkireddy, S., Agrawal, Y.K., 2017.
553 Development of a novel "nanocarrier" system based on Halloysite Nanotubes to overcome the
554 complexation of ciprofloxacin with iron: An in vitro approach. Appl. Clay Sci. 150, 293-302.
555 Riela, S., Massaro, M., Colletti, C.G., Bommarito, A., Giordano, C., Milioto, S., Noto, R., Poma, P.,
556 Lazzara, G., 2014. Development and characterization of co-loaded curcumin/triazole-halloysite
557 systems and evaluation of their potential anticancer activity. Int. J. Pharm. 475, 613-623.
558 Sabbagh, N., Akbari, A., Arsalani, N., Eftekhari-Sis, B., Hamishekar, H., 2017. Halloysite-based
559 hybrid bionanocomposite hydrogels as potential drug delivery systems. Appl. Clay Sci. 148, 48-55.

560   Sadjadi, S., Atai, M., 2018. Ternary hybrid system of halloysite nanotubes, polyacrylamides and
561   cyclodextrin: an efficient support for immobilization of Pd nanoparticles for catalyzing coupling
562   reaction. Appl. Clay Sci. 153, 78-89.
563   Sdiri, A., Khairy, M., Bouaziz, S., El-Safty, S., 2016. A natural clayey adsorbent for selective
564   removal of lead from aqueous solutions. Appl. Clay Sci. 126, 89-97.
565   Silva, R.T.D., Pooria, P., Goh, K.L., Chai, S.P., Chen, J., 2013. Synthesis and characterisation of
566   poly (lactic acid)/halloysite bionanocomposite films. J. Compos. Mater. 48, 3705-3717.
567   Tan, D., Yuan, P., Liu, D., Du, P., 2016. Surface Modifications of Halloysite, in: Yuan, P., Thill,
568   A., Bergaya, F. (Eds.), Nanosized Tubular Clay Minerals - Halloysite and Imogolite. Elsevier, pp.
569   167-201.
570   Uddin, M.K., 2017. A review on the adsorption of heavy metals by clay minerals, with special focus
571   on the past decade. Chemical Engineering Journal 308, 438-462.
572   Yuan, P., Southon, P.D., Liu, Z., Green, M.E.R., Hook, J.M., Antill, S.J., Kepert, C.J., 2008.
573   Functionalization of Halloysite Clay Nanotubes by Grafting with γ-Aminopropyltriethoxysilane. J.
574   Phys. Chem. C 112, 15742-15751.
575   Yuan, P., Southon, P.D., Liu, Z., Kepert, C.J., 2012. Organosilane functionalization of halloysite
576   nanotubes for enhanced loading and controlled release. Nanotechnology 23, 375705.
577   Yuan, P., Tan, D., Bergaya, F.A., 2015. Properties and applications of halloysite nanotubes: recent
578   research advances and future prospects. Appl. Clay Sci. 112-113, 75-93.
579   Zeng, G., He, Y., Zhan, Y., Zhang, L., Pan, Y., Zhang, C., Yu, Z., 2016. Novel polyvinylidene
580   fluoride nanofiltration membrane blended with functionalized halloysite nanotubes for dye and
581   heavy metal ions removal. J. Hazard. Mater. 317, 60-72.
582   Zhao, Y., Abdullayev, E., Vasiliev, A., Lvov, Y., 2013. Halloysite nanotubule clay for efficient
583   water purification. J. Colloid Interf. Sci. 406, 121-129.
584   Zhu, K., Duan, Y., Wang, F., Gao, P., Jia, H., Ma, C., Wang, C., 2017. Silane-modified
585   halloysite/Fe3O4 nanocomposites: Simultaneous removal of Cr(VI) and Sb(V) and positive effects
586   of Cr(VI) on Sb(V) adsorption. Chem. Eng. J. 311, 236-246.
587
588

589